

Shape Deformations in Atomic Nuclei

Ikuko Hamamoto^{1,2,3} and Ben R. Mottelson^{2,4}

¹ *Division of Mathematical Physics,*

Lund Institute of Technology at the University of Lund,

Lund, Sweden

² *The Niels Bohr Institute,*

Blegdamsvej 17, Copenhagen Ø,

DK-2100, Denmark

³ *Riken Nishina Center, Wako,*

Saitama, 351-0198 Japan

⁴ *NORDITA, Blegdamsvej 17,*

Copenhagen Ø, DK-2100, Denmark

PACS numbers:

The ground states of some nuclei are described by densities and mean fields that are spherical, while others are deformed. The existence of non-spherical shape in nuclei represents a spontaneous symmetry breaking.

I. INTRODUCTION

The low energy spectra of many nuclei can be described by independent particle motion in a mean field potential that has spherical symmetry, but the spectra of many others are most simply described by a mean field that deviates significantly from spherical symmetry. Figure 1 presents the regions of neutron and proton particle numbers (N, Z) where these deviations (*i.e.* deformations) have been empirically observed. The existence of deformation is made apparent by the related physical phenomena: (i) Electric quadrupole moments¹ and rates for electromagnetic quadrupole transitions that are orders of magnitude larger than can be accounted for by the estimates for quantum transitions of a single proton. (ii) The low energy spectrum contains sequences of excited states with consecutive values of the quantized angular momentum, I , with associated excitation energy varying as $I(I + 1)$ (as is known for the rotational kinetic energy of molecules). (iii) In addition to the rotational excitations the spectra exhibit low-energy single-particle excitations that can be interpreted in terms of particles moving independently in a potential with spheroidal shape.

The occurrence of deformation is a prerequisite to collective rotation of a quantum system because otherwise one cannot speak of an orientation for the system. All molecules are deformed because they are built from a (small) number of atoms which unavoidably break the rotational symmetry of the system. The close connection of deformation and rotation is not only crucial in the understanding of nuclear structure, but also at once allies this project with a wide range of currently studied man-made finite systems as clusters of atoms, quantum dots, and trapped cold atomic gases.

II. PHYSICS AND GEOMETRY OF BROKEN ROTATIONAL SYMMETRY

The nuclear many-body Hamiltonian involves kinetic energy that does not depend on the orientation of the coordinate axes together with interactions that depend on the relative coordinates of the particles and therefore is also invariant under rotations of coordinate axes involving all of the particles at once. This rotational symmetry does not however exclude the possibility of finding that the lowest-energy mean field solution is obtained with

¹ Electric quadrupole moment is defined in eq. (11) and is a measure of the simplest deviation from spherical symmetry in the nuclear density distribution.

a non-spherical mean potential and density distribution. The non-spherical solutions are interpreted as deformed intrinsic states. The occurrence of rotational spectra implies an approximate separation of the collective rotation as a whole from the intrinsic motion in the body-fixed system as described by a Hamiltonian

$$H = H_{int} + H_{rot} \quad (1)$$

where the mean field of H_{int} is non-spherical. Then, the total wave function Ψ can be written, in the first approximation, as

$$\Psi = \phi_{int}(q) \Phi_{rot}(\Omega) \quad (2)$$

where the variables q describe the motion of the individual neutrons and protons with respect to an intrinsic (body fixed) coordinate system while Ω describes the orientation of the latter system with respect to the laboratory. (See Figures 2 and 3.) A general discussion of the form of H_{rot} can be found in the Chapter 4 of [1] or in the section 3.3 of [4].

The origin of nuclear deformations can be related to the shell structure of single-particle levels (*i.e.* the bunching of single-particle energy levels) in a spherical potential. The occurrence of significant gaps in the level spacing at the major shell closures provides the rational for the special stability of these nuclei and at the same time implies that the single-particle level density in the middle of the shell for a spherical mean field is appreciably greater than the over-all average. All single-particle wave functions in the spherical potential (except for $p_{1/2}$ and $s_{1/2}$) have a large intrinsic anisotropy and thus in the presence of a deformed one-particle potential some single particle orbits will move up in energy and others will move down as a function of deformation. This fanning out of the one-particle energies implies that the excessive one-particle level density in the middle of closed shells is relaxed. Thus, the filling of the lowest orbits may provide an energy gain stabilizing the deformed configuration. The eccentricities obtained in this way for nuclear ground states are small compared with unity, reflecting the fact that the number of particles in open shells is small compared with the total ($A = N + Z$).

The existence of non-spherical shape in nuclei represents a spontaneous symmetry breaking and the rotational excitations are the Goldstone mode for this symmetry breaking. The full rotational degrees of freedom² are obtained if the deformation completely breaks the

² This implies $(2I + 1)^2$ different rotational states for each value of I .

rotational symmetry (Figure 2). However, if the deformation is invariant with respect to a subgroup of rotations of the coordinate frame, the collective rotational degree of freedom is correspondingly restricted. For example, if the deformation is axially symmetric, the rotation about the symmetry axis does not belong to collective rotation, but is part of the intrinsic particle or vibrational degrees of freedom³ (Figure 3).

The symmetry of deformation restricts the quantum numbers of the rotational spectra. Examples are ; (a) Space reflection invariance of deformation leads to parity as a good quantum number in the rotational spectra, *i.e.* all members in a given rotational band have the same space inversion parity, $\pi = \pm 1$. (b) Axially symmetric shape in quantum mechanics implies no collective rotation about the symmetry axis and that the intrinsic motion has a constant projection of angular momentum K on the symmetry axis. Consequently, the projection, K , of the total angular momentum along the symmetry axis is a good quantum number which is common to all members of the rotational band. (c) When the deformation has R -symmetry (*i.e.* invariant with respect to a rotation of 180° about an axis perpendicular to the symmetry axis) in addition to axial symmetry, for example a deformation depending on the spherical harmonic $Y_{\lambda 0}$ with even λ , the $K=0$ states are eigenstates of the R -operator with eigenvalues $r = \pm 1$. The observed rotational bands comprise only the states

$$I = \begin{cases} 0, 2, 4, \dots & \text{for } K = 0, r = + \\ 1, 3, 5, \dots & \text{for } K = 0, r = - \end{cases} \quad (3)$$

$$I = K, K + 1, K + 2, \dots \quad \text{for } K \neq 0 \quad (4)$$

implying uniquely R -symmetry for these deformed nuclei. In the case of $K \neq 0$ the total wave functions take the form

$$\Psi_{KIM} = \left(\frac{2I+1}{16\pi^2} \right)^{1/2} \left(\phi_K(q) D_{MK}^I(\Omega) + (-1)^{I+K} \phi_{\bar{K}}(q) D_{M,-K}^I(\Omega) \right) \quad (5)$$

in order to fulfill the condition that the rotation by 180° about an axis perpendicular to the symmetry axis is part of the intrinsic degrees of freedom and should not be included in the rotational degrees of freedom [1]. In Eq. (5) M denotes the component of \mathbf{I} along the z-axis of a coordinate system fixed in the laboratory, while the intrinsic state $\phi_{\bar{K}}(q)$ is

³ There are now $(2I+1)$ different rotational states for each value of $I \geq |K|$ where K is a constant intrinsic quantum number characterizing the rotational band.

the time-reversed state of $\phi_K(q)$ or $\phi_{\bar{K}}(q) \equiv R_i^{-1}\phi_K(q)$ where R_i expresses the operator R acting on the intrinsic variables. The rotation matrices D_{MK}^I depend on the orientation of the intrinsic coordinate system with respect to the laboratory and are given in the standard textbooks [2].

The symmetrization (5) of the $K \neq 0$ states leads to additional terms in the rotational energy and intensity rules for these states. For example, for $K=1/2$ the rotational energy to leading-order in the angular momentum acquires an additional term

$$E_{rot} = A \left(I(I+1) + a(-1)^{I+1/2} \left(I + \frac{1}{2} \right) \delta(K, \frac{1}{2}) \right) \quad (6)$$

where the parameter, $a = - < K = 1/2 | j_+ | R_i^{-1} (K = 1/2) >$, is referred to as the decoupling parameter while \mathbf{j} is the angular momentum of the single particle in the $\Omega=1/2$ state if the $K=1/2$ can be associated with a single particle moving in the potential generated by the rotating core. Writing $A = \hbar^2/2\mathfrak{I}$, \mathfrak{I} is the effective moment of inertia of the band.

In contrast to the symmetry, the size of deformation is related to the magnitudes of rotational energy (or moment of inertia) and E2 transition probability (or intrinsic quadrupole moment).

With only a single exception the observed rotational states (see for example Figures 4, 6 and 8) exhibit only the subset of the states identified in (5), which uniquely identifies the existence of both axial- and R -symmetry for these states, and in the rest of this article we shall confine the discussion to this case; for a more general discussion see Ref. [1]. For the only known example, so far, of a nucleus clearly exhibiting triaxial shape, see wobbling mode in Section VII.

III. MOMENT OF INERTIA FOR NUCLEAR ROTATION

The theory for the moment of inertia is based on the analysis of the extra kinetic energy that is generated when the self-consistent deformed mean-field potential is adiabatically set into uniform rotation with frequency $\vec{\omega}_{rot}$ about an axis perpendicular to the intrinsic symmetry axis. The Coriolis force, which is associated with this rotation and couples intrinsic motion with rotation, generates the moment of inertia as the second order perturbation effect [3] of the single-particle angular-momentum operator, $j_x(k)$, acting on the non-rotating

ground state, $|0\rangle$.

$$\mathfrak{S}_x = 2\hbar^2 \sum_{i \neq 0} \sum_{k=1}^A \frac{\langle i | j_x(k) | 0 \rangle^2}{E_i - E_0} \quad (7)$$

where i labels the many-particle states of the A nucleons in the deformed potential, with excitation energies E_i . For non-interacting nucleons moving in the deformed mean field, the semi-classical evaluation of (7) leads, most amazingly, to a moment of inertia equal to the value obtained for rigid rotation of a body with the given mass density distribution⁴, which is to leading order in the deformation

$$\mathfrak{S}_{x,rig} = A M \langle y^2 + z^2 \rangle = \frac{2}{5} A M R^2 \left(1 + \frac{1}{3}\delta\right) \quad (8)$$

assuming axial symmetry about the intrinsic z-axis, where R is the mean radius, A denotes the mass number, M the nucleon mass, while δ is the deformation parameter determined from the electric quadrupole moment in (11).

Moments of inertia observed in the ground state bands of well-deformed even-even nuclei are systematically a factor of 2-3 smaller than the values for rigid rotation of the deformed body (\mathfrak{S}_{rig}), revealing a significant violation of the assumed independent particle motion of the single particles. The correlations revealed by the effect have been understood in terms of a pair binding of the same kind as that involved in the Bardeen, Cooper, and Schrieffer (BCS) theory of superconductivity⁵. The pair gap, Δ , in the BCS theory is identified with the pair binding observed in the systematically larger binding energies of nuclei with even number of neutrons or protons as compared with the neighboring nuclei having an odd number of the same (see the scholarpedia article on pair correlations in nuclei). The presence of the pair gap increases the energy denominators and reduces the matrix elements in the numerators in the cranking calculation of the moments of inertia (7) for the ground states

⁴ The result, $\mathfrak{S}_x \rightarrow \mathfrak{S}_{x,rig}$, is based on a classical argument first found in Niels Bohr's doctoral dissertation [5] and usually referred to in the condensed matter literature as the Bohr-van Leeuwen theorem. Since the first-order effects of the rotation are equivalent to the effect of a magnetic field, the absence of an induced flow in the rotating coordinate system corresponds to the absence of diamagnetism in a classical electron gas. In the case of an anisotropic harmonic oscillator potential the rigid-body value of non-interacting nucleons is just obtained for the equilibrium deformation independent of configurations. (The closed-shell configurations are a singular exception to this result, since they have spherical equilibrium shape and a vanishing moment of inertia.) For other potentials one obtains fluctuations of the moment of inertia about the rigid-body value depending on configurations [6].

⁵ The concepts developed for the treatment of superconductivity in terms of correlations in the electronic motion [7] provided a basis for analyzing the pair correlation in nuclei [8]. See also Ref. [9]

of even-even nuclei and reproduces rather well the main trends in the empirical moments for the even-even nuclei, see Ref. [10].

Although the BCS correlations appear to provide the beginning of an understanding of the nuclear moments of inertia, the particle-rotational coupling continues to challenge our understanding since in the odd-A nuclei the same Coriolis perturbation that generates the moments of inertia couples near-lying rotational bands with $\Delta\Omega = \pm 1$, where Ω represents the component of the total angular momentum along the symmetry axis, and produces observable effects in the rotational energies and E2 transition probabilities. The observed perturbations are systematically smaller by an appreciable factor than for uncorrelated single particle motion, but in this case the BCS pair correlations provide only a minor reduction (10-20 percent) leaving the observed perturbation unexplained. This "Coriolis reduction" problem is still an open issue.⁶

IV. DEFORMATION AND ROTATIONAL BAND IN THE SU_3 MODEL

The variables that describe the collective rotational motion are in general complicated functions of both the particle positions and momenta. Taking the particle motion within one-major shell of a harmonic oscillator potential, the relationship between collective rotation and individual-particle motion is clarified in the SU_3 model [11]. In the historical development the SU_3 model was a wonderful and liberating contribution towards understanding the manner in which interacting particles within a single major shell could produce deformation and associated rotational band structure in the excitation spectrum.

For a system with n nucleons the eight SU_3 operators consist of three rotation operators

$$L_q = \sum_{k=1}^n (\mathbf{r}(k) \times \mathbf{p}(k))_q \quad (9)$$

and five quadrupole operators

$$Q_q^{(2)} = \sqrt{\frac{4\pi}{5}} \sum_{k=1}^n \left(r(k)^2 Y_q^{(2)}(\theta_r(k), \phi_r(k)) + b^4 p(k)^2 Y_q^{(2)}(\theta_p(k), \phi_p(k)) \right) \frac{1}{b^2} \quad (10)$$

where b is the radial length parameter of the harmonic-oscillator wave functions while the arguments of the spherical harmonics are the polar angles of the vectors \mathbf{r} and \mathbf{p} , respectively.

⁶ See F. Stephens (1960) quoted in Ref. [1]. Detailed discussions can be found in p.250-253, p.279, p.314 and p.318 of Ref. [1].

The oscillator Hamiltonian, $H_0 = r^2 + b^4 p^2$, is invariant with respect to the above eight operators. The presence of the momentum-dependent term in $Q_q^{(2)}$ ensures that there is no mixing of different oscillator configurations. Single-particle wave functions belonging to given irreducible representations of the SU_3 group are eigenfunctions of H_0 as well as being eigenfunctions of Q_0 . Thus, they may be regarded as approximations to the wave functions of a deformed oscillator potential obtained by neglecting the mixing of different oscillator shells N . Noting that the Casimir operator which is quadratic in the group operators is written as $C = \frac{1}{4}(\mathbf{Q}^{(2)} \cdot \mathbf{Q}^{(2)})_0 + \frac{3}{4}(\mathbf{L} \cdot \mathbf{L})_0$, the eigenvalues of the quadrupole-quadrupole force within the SU_3 multiplet form a set of rotational bands with energies proportional to $L(L+1)$.

It is possible to construct the wave functions, which may be interpreted as intrinsic wave functions, for a given irreducible representation which in general includes several intrinsic wave functions. Then, the set of wave functions which are obtained from a given intrinsic state by projecting all possible values of angular momentum forms an SU_3 multiplet. The multiplet with the greatest deformation lies lowest in energy with an attractive quadrupole force. It is important to notice the presence of a particle-hole symmetry in the SU_3 model, which leads to the number of prolate systems equal to that of oblate ones for the nuclear ground states. One expects prolate intrinsic shapes in the first half-shell and oblate intrinsic shapes in the second half. If the electric quadrupole operator is proportional to the group operator $\mathbf{Q}^{(2)}$, it has non-vanishing matrix elements only between states in the same SU_3 irreducible representation. Such transitions exhaust all the strength of the E2 transitions.

Thus, the SU_3 classification provides an exact microscopic model in which a quadrupole-quadrupole force leads to a ground state with large quadrupole moment. Moreover, not only the energy spectrum but also quadrupole transition probabilities have rotational characteristics in the limit of many particles and not near the top of the band, where there is a band termination accompanied by a smooth decrease in the E2 transition matrix-element reaching $B(E2; I_{max} \rightarrow I_{max} + 2) = 0$ where I_{max} is the largest angular momentum in the band. Since the maximum angular momentum of the single-particle and the number of particles in the last filled shell are the order of $A^{1/3}$ and $A^{2/3}$, respectively, the rotational bands terminate at an angular momentum of order A reflecting the finite dimensionality of the shell model space involved. Having the results of the SU_3 model in mind, in the following section we build the concepts of deformation and rotation directly from broken rotational symmetry

and a resulting intrinsic state.

V. SINGLE-PARTICLE STATES IN DEFORMED NUCLEI

In the regions of particle number where the even-even nuclei exhibit rotational band structure (Figure 1), the low energy spectra of the neighboring odd-A nuclei can be interpreted in terms of rotational sequences based on the different single particle or single hole states in the Fermi sea of particle orbits in an appropriately chosen spheroidal potential. Expressing a projection of the angular momentum of the last odd particle by Ω , observed values of $K\pi$ for the lowest bands are equal to respective values of $\Omega\pi$, and the wave function of the odd particle is conveniently used for the intrinsic wave function $\phi_K(q)$ in (5); Examples are provided by observed spectra in Figures 6 and 8 which are interpreted on the basis of the theoretical spectra in Figures 7 and 9.

The rotational coupling scheme between intrinsic and rotational angular momenta is confirmed not only by the sequence of spin values and regularities in the energy spectra, but also by the intensity relations that govern the transitions between states within a given band as well as those between two rotational bands [1]. The leading order intensity rules are of a purely geometrical character depending only on the rotational quantum numbers and the multipolarity of the transitions.

The starting point for the description of the intrinsic degrees of freedom is the analysis of single-particle motion in non-spherical potentials with the symmetry and shape exhibited by the observed rotational spectra. The theoretical energy spectrum of one-particle eigenvalues plotted as a function of the axially-symmetric quadrupole deformation parameter is referred to as the Nilsson diagram [12]. The presence of a significant pairing correlation in the nuclear system (as observed in the odd-even mass difference) implies that the low energy odd-A spectra are especially simple and for deformed nuclei can be completely interpreted in terms of a single quasiparticle occupation of the Nilsson diagram orbits lying in the neighborhood of the Fermi energy.

There are several definitions which have been conventionally used for the parameter of axially-symmetric quadrupole (Y_{20}) deformation. Assuming a collective deformation of the

nucleus as a whole, δ is defined using the intrinsic electric quadrupole moment

$$Q_0 = \sum_{k=1}^Z \langle 2z_k^2 - x_k^2 - y_k^2 \rangle = \frac{4}{3} \langle \sum_{k=1}^Z r_k^2 \rangle \delta \quad (11)$$

while β is defined in terms of the expansion of the radius parameter

$$R(\theta, \varphi) = R_0 (1 + \beta Y_{20}^*(\theta) + \dots) \quad (12)$$

where R_0 is obtained by assuming a constant density for the undistorted spherical shape.

To leading order, one obtains $\beta = \delta \sqrt{\frac{16\pi}{45}} \approx 1.06 \delta$.

The single-particle spectrum for an axially-symmetric harmonic-oscillator potential

$$V_{def.h.o.} = \frac{M}{2} (\omega_z^2 z^2 + \omega_\perp^2 (x^2 + y^2)) \quad (13)$$

is plotted in Figure 5. Note that in the potential (13) there is neither surface nor spin-orbit potential, though both of these are important in actual nuclei. The lowest (highest) orbit for prolate (oblate) shape is doubly degenerate ($n_\perp = 0$) and has an axially-symmetric density distribution, which is built by taking a linear combination of the one-particle orbits degenerate for spherical shape, while the density distributions of other one-particle orbits are in general not axially-symmetric. In the absence of two-body interactions the configurations with an unfilled shell in the harmonic oscillator potential have always a deformed equilibrium shape. For example, the two-particles (two-holes) configuration in a given $N \neq 0$ shell of the harmonic oscillator potential has an equilibrium deformation of prolate (oblate) shape.

It is seen that the strongest bunching of levels in Figure 5 occurs for spherical shape but a similar order of level bunching occurs for large deformations with simple rational ratios of $\omega_\perp : \omega_z$. For large deformations such as 2 : 1 ($\delta_{osc} = 0.6$) or 1 : 2 ($\delta_{osc} = -0.75$) a shell structure which is essentially different from that for spherical shape appears. These deformations have not been observed in the ground state of heavy nuclei, but observed fission isomers in actinide nuclei [13] and "superdeformed" yrast bands [14] at high spins of some medium-heavy nuclei are understood in terms of the prominent shell structure and the associated magic numbers that occur for $\omega_\perp : \omega_z = 2 : 1$ (superdeformation) in the harmonic oscillator potential.

An example of observed well-studied low-energy spectra of deformed odd-A nuclei is shown in Figure 6. The observed spectra can be understood in terms of the "aligned" coupling scheme, in which the orbital motion of nucleons is aligned with respect to the

orientation of the deformed field as illustrated in Figure 3. In this example the ground state configuration ($K^\pi = 0^+$) of ${}^{24}_{12}\text{Mg}_{12}$ is characterized by the pairwise filling of the time-reversed orbits aligned with respect to the symmetry axis while the 13th neutron of ${}^{25}_{12}\text{Mg}_{13}$ moves in the spheroidal potential provided by the even-even core of ${}^{24}\text{Mg}$. Both energies and I^π quantum numbers of the observed states are successfully classified in terms of rotational bands characterized by the quantum numbers K^π , which correspond to the values of Ω^π of the odd neutron for a prolate deformation with $\beta \approx 0.4$. An example of the corresponding Nilsson diagram based on a spheroidal Woods-Saxon plus spin-orbit potential is shown in Figure 7.

In the classification of observed levels shown in Figure 6 we have used the fact that the levels (with $\Delta I \leq 2$) belonging to the same rotational band must be connected by strongly enhanced (collective) E2 transitions. Using the wave function in (5) the reduced E2 transition probabilities within a band are written as

$$B(E2; KI_1 \rightarrow KI_2) = \frac{5}{16\pi} e^2 Q_0^2 \langle I_1 K 20 | I_2 K \rangle^2 \quad (14)$$

where $\langle I_1 K 20 | I_2 K \rangle$ is a Clebsch-Gordan coefficient, while Q_0 expresses the intrinsic electric quadrupole moment. The value $\beta \approx 0.4$ is extracted from the Q_0 value which is obtained by analyzing measured strong E2 transitions within a given rotational band. Thus, the extracted β -value is consistent with that obtained from the comparison of the assigned K^π values of the observed bands with the Ω^π values of one-particle orbits in the Nilsson diagram of Figure 7. The analysis of other available data, M1/E2 transitions, β decays and one-nucleon transfer reactions, has been carried out in a similar manner and provides further support to the interpretation based on the Nilsson diagram [1].

The analysis of available experimental data on medium-heavy deformed odd-A nuclei based on the Nilsson diagram, in which the pair correlation becomes important and has to be taken into account in addition to the spheroidal potential, has been even more quantitatively successful. In those heavier nuclei the notion of the deformed mean field is theoretically better justified; however, due to the higher density of one-particle levels the Nilsson diagram appropriate for those nuclei becomes more complicated. A beautiful example of observed data is shown in Figures 8 and interpreted in terms of the Nilsson diagram given in figure 9. We refer the reader to many other such examples in the text book [1].

VI. THE YRAST LINE

The yrast line is defined by the quantum state with the lowest energy for a given angular momentum. In the yrast region the nucleus is cold in the sense that the entire excitation energy of the nucleus is exhausted in generating the large total angular momentum. Therefore, the structure in the yrast region is expected to be ordered with simple excitation modes characteristic of the approach to zero temperature, and the study of quantal spectra in this region may be expected to give important nuclear-structure information on how the nucleus responds to the large centrifugal forces associated with rotation.

The path that the yrast line of actual nuclei will follow in deformation space with increasing angular momentum will result from the interplay of the macroscopic centrifugal distortion effect and quantal effects associated with shell structure. A typical example of quantal effects is the observation of superdeformed bands ($\delta \approx 0.6$) in nuclei with certain proton and neutron numbers along the high-spin yrast line [15]. With the singular exception of ^8Be superdeformation has not been seen in any nuclear ground state, but along the yrast line, the exceptionally large moment of inertia associated with these large deformations provides the explanation for the extensive regions where superdeformation is observed at high angular momentum on the yrast line [14]. The yrast configurations in some nuclei accommodate the angular momentum by collective motion giving rise to regular sequences of levels (along a band as in molecules), while those in other nuclei correspond to rearrangements of the orbits of single or a few nucleons (involving a transition to a new band). The shape change along the yrast line and the related phenomena, which have been explored, may be conveniently found in various review articles [16] and conference proceedings [17].

The maximum value of the angular momentum that can be accommodated by a nuclear system is limited by the fission instability (in heavier nuclei) or by the ejection of particles carrying large orbital angular momentum (in lighter nuclei).⁷

When the coupling scheme along the yrast line is such that the angular momentum is oriented approximately in the direction of the symmetry axis of oblate shape, each one-

⁷ A very different collective mode for generating states with large angular momentum is provided by the possibility of creating vortices in the quantum fluid. However, already a single vortex carries an angular momentum, $\hbar L$, of order of the number of particles, A , and thus can only occur in finite systems that are constrained by external force fields, as for example in the high angular-momentum states of electrons in atoms.

particle orbit contributes a definite angular momentum in the direction of the rotation axis. Then, the transitions along the yrast line involve successive rearrangements in the occupation of one-particle orbits. In other words, the collective moments of inertia are so small that each band contributes only a single state to the yrast sequences. Consequently, the energies on the yrast line may exhibit considerable irregularity, and the transitions are at most of one-particle strength and may suffer considerable hindrance which may lead to the occurrence of yrast traps (yrast isomers).

The manner of rotation together with the intrinsic deformation in a band may change as I increases. As rotation sets in, the yrast shape of nuclei may become triaxial (*i.e.* $R_x \neq R_y \neq R_z$) at a critical rotational frequency, and rotational bands may terminate at some angular momentum as in the SU_3 model, when the angular momentum I is built up by a finite number of nucleons in a given open shell. Approaching to the termination of the band is exhibited by a decrease of the probabilities of E2 transitions within the band, since the gradual alignment of the nucleons leads towards a density distribution that is more and more symmetric about the axis of rotation [1]. On the other hand, bands may not terminate if excited configurations start to mix smoothly into rotational levels as I increases. The latter has been shown to occur when the deformation of the band is larger than some critical value [18].

VII. MISCELLANEOUS

We mention briefly seven topics concerning shape deformations which were not included in the previous sections: (i) the magic numbers ($N, Z = 8, 20, 28, 50, 82, 126, \dots$) traditionally known in stable nuclei may change in nuclei away from the stability line. The change in drip-line quantum-numbers comes from the presence of weakly-bound nucleons (especially neutrons due to the absence of a Coulomb barrier), which leads to a change in shell-structure around the Fermi level. The neutron drip line has so far been experimentally reached in the oxygen ($Z=8$) isotope, for which ${}^{24}_{8}\text{O}_{16}$ is the heaviest element inside the drip line. Some neutron-drip-line nuclei with a traditional magic number of neutrons such as $N = 8$ and 20 (for example, ${}^{12}_4\text{Be}_8$ [19] and ${}^{30}_{10}\text{Ne}_{20}$ [20]) are indeed found to have prolate ground-state deformation. (ii) It is now widely observed that a given nucleus accommodates various shapes depending on excitation energies and spins. Even-even nuclei with closed-shell ground

states exhibit excited states with strongly deformed shape and rotational spectra. For example, $^{16}_8\text{O}_8$ (the rotational band beginning at 6.05 MeV) and $^{40}_{20}\text{Ca}_{20}$ (at 5.21 MeV) [21]. (iii) The observation of wobbling mode in the neutron-deficient nucleus $^{163}_{71}\text{Lu}_{92}$ at moderate spins [22, 23] manifests the presence of triaxial quadrupole deformed shape in nuclei. The characteristic feature of the wobbling mode has been pinned down by the detailed study of the electromagnetic properties. (iv) The observed almost complete dominance of prolate over oblate deformations in the ground states of deformed even-even nuclei is not yet adequately understood. (v) The observation of remarkably low frequency negative-parity excitations in some even-even actinide nuclei (for example, the $I^\pi = 1^-$ state observed at 0.216 MeV in $^{224}_{88}\text{Ra}_{136}$ [24]) indicates an incipient octupole instability in this nucleus. (vi) It is remarked that presently available self-consistent mean-field approximation to the nuclear many-body Hamiltonian with effective interactions gives a good description of the observed regions of quadrupole-deformed nuclei [25], though observed prolate dominance is unresolved. For a discussion of the quadrupole correlation effect described by the generator coordinate method, see [26]. On the other hand, shell-model calculations of conventional type are not quantitatively successful in studying the properties of deformed nuclei except for light nuclei, basically because the configuration space must be truncated in order to be able to carry out the calculation. A recent development of the shell-model technique in the study of deformed nuclei can be found in [27]. (vii) In a quantal system such as nuclei, the definition of deformation requires the condition that the zero-point shape fluctuations are small compared with the equilibrium deformation values. The distribution of the ratio $R = E(4_1^+)/E(2_1^+)$ observed in even-even nuclei has a sharp peak around $R = 3.3$, which indicates an axially-symmetric rotor with a very weak coupling to intrinsic motion. Available systematic microscopic calculations suggest the relatively rigid shape of these deformed nuclei [28].

As a final remark, we may mention; (a) the construction of facilities providing radioactive ion beams has in recent years made (and will make) it possible to reach out to the region of the nuclear chart further away from stability; (b) the remarkable development of the advanced 4π γ -ray detector systems has led to the observation of weakly-populated states of exotic shapes and/or extreme angular momentum.

-
- [1] A. Bohr and B. R. Mottelson, *Nuclear Structure* (Benjamin, Reading, MA, 1975), Vol.II.
 - [2] For example, M. E. Rose, *Elementary Theory of Angular Momentum* (Wiley and Sons, New York, 1957).
 - [3] D. R. Inglis, Phys. Rev. **96**, 1059 (1954).
 - [4] P. Ring and P. Schuck, *The nuclear many-body problem* (Springer-Verlag, New York, Heidelberg, Berlin, 1980).
 - [5] N. Bohr, *Studier over Metallernes Elektrontheori*, dissertation, Thaning og Appel, Copenhagen, 1911; transl. in *Niels Bohr, Collected Works*, vol. 1, p.291, ed. J. Rud Nielsen, (North-Holland, 1972).
 - [6] A. Bohr and B. R. Mottelson, Mat. Fys. Medd. Dan. Vid. Selsk. **30**, no. 1 (1955).
 - [7] J. Bardeen, L. N. Cooper and J. R. Schrieffer, Phys. Rev. **106**, 162 and **108**, 1175 (1957).
 - [8] A. Bohr, B. R. Mottelson and D. Pines, Phys. Rev. **110**, 936 (1958).
 - [9] S. T. Belyaev, Mat. Fys. Medd. Dan. Vid. Selsk. **31**, no. 11 (1959).
 - [10] S. G. Nilsson and O. Prior, Mat. Fys. Medd. Dan. Vid. Selsk. **32**, no. 16 (1961); J. J. Griffin and M. Rich, Phys. Rev. **118**, 850 (1960).
 - [11] J. P. Elliott, Proc. Roy. Soc. (London), **A245**, 128 and 562 (1958).
 - [12] S. G. Nilsson, Mat. Fys. Medd. Dan. Vid. Selsk. **29**, no. 16 (1955).
 - [13] A. Michaudon, Advances in Nuclear Physics, **6**, 1, eds. M.Baranger and E. Vogt, (Plenum Press, New York, N. Y., 1973).
 - [14] R. V. F. Janssens and T. L. Khoo, Ann. Rev. Nucl. Part. Sci. **41**, 321 (1991).
 - [15] P. Twin *et al.*, Phys. Rev. Lett. **57**, 811 (1986).
 - [16] For example, J. D. Garrett, G. B. Hagemann and B. Herskind, Ann. Rev. Nucl. Part. Sci. **36**, 419 (1986); I. Hamamoto, *Treatise on Heavy-Ion Science*, vol. **3**, ed. D. A. Bromley, (Plenum, 1985).
 - [17] For example, Proc. of International Seminar on "The frontier of nuclear spectroscopy", eds. Y. Yoshizawa, H. Kusakari and T. Otsuka, (World Scientific, 1993); Nucl. Phys. **A520**, 1c-745c (1990) and **A557**, 1c-753c (1993).
 - [18] T. Troudet and R. Arvieu, Z. Physik **A291**, 183 (1979).
 - [19] H. Iwasaki *et al.*, Phys. Lett. **B481**, 7 (2000) and **B491**, 8 (2000).

- [20] Y. Yanagisawa *et al.*, Phys. Lett. **B566**, 84 (2003).
- [21] E. Ideguchi *et al.*, Phys. Rev. Lett. **87**, 222501 (2001).
- [22] S. W. Ødegård *et al.*, Phys. Rev. Lett. **86**, 5866 (2001).
- [23] D. R. Jensen Phys. Rev. Lett. **89**, 142503 (2002).
- [24] F. Stephens, F. Asaro and I. Perlman, Phys. Rev. **96**, 1568 (1954).
- [25] For example, D. Vautherin, Phys. Rev. **C7**, 296 (1973); References quoted in M. Bender, P.-H. Heenen and P.-G. Reinhard, Rev. Mod. Phys. **75**, 121 (2003).
- [26] M. Bender, G. Bertsch and P.-H. Heenen, Phys. Rev. **C73**, 0343221 (2006).
- [27] E. Caurier *et al.*, Rev. Mod. Phys. **77**, 427 (2005).
- [28] For example, J.-P. Delaroche *et al.*, Phys. Rev. **C81**, 014303 (2010).
- [29] A. Bohr and B. R. Mottelson, *Nuclear Structure* (Benjamin, Reading, MA, 1969), Vol.I.

Figure captions

Figure 1 : Regions of deformed nuclei. The nuclei, for which both N and Z are even numbers (called even-even nuclei), have ground-state spin-parity 0^+ , without exception. The overwhelming majority of these has 2^+ first excited state. Writing the excitation energies of the lowest-lying 2^+ and 4^+ states as $E(2_1^+)$ and $E(4_1^+)$, the filled circle represents even-even nuclei, in which $E(4_1^+)/E(2_1^+) > 2.7$. The data are taken from <http://www.nndc.bnl.gov/ensdf/>. The line of β stability is indicated by the thin long-dashed curve. The thin straight lines parallel to the x and y axes show the magic numbers of protons and neutrons, which are known in nuclei along the β stability line. Except for very light nuclei ($Z \leq 8$) the neutron drip line, at which nuclei become unstable for neutron emission, is not known experimentally. The boarder of deformed nuclei shown for the neutron-rich region of medium-heavy nuclei is often equal to the boarder of neutron-rich nuclei, for which the energy of the 4_1^+ state is presently known. The criterion of deformed even-even nuclei can be made in one of the following four ways; (i) the excitation spectra exhibit an approximate $I(I+1)$ energy dependence indicating rotational structure. In the figure the (rather arbitrary) criterion $E(4_1^+)/E(2_1^+) > 2.7$ is chosen. (ii) $B(E2)$ values are much larger than single particle or collective vibrational estimates. (iii) The excitation energy of the first excited 2^+ state is especially low, say by a factor of at least 5, compared with twice the odd-even mass difference, 2Δ . We note that the ratio, $E(2_1^+)/2\Delta$, has the mass-number dependence of about $A^{1/6}$. (iv) The ratio, $Q(2_1^+)^2/B(E2; 2_1^+ \rightarrow 0_{gr}^+)$, where $Q(2_1^+)$ expresses the quadrupole moment of the lowest 2^+ state while $B(E2)$ denotes the reduced probability of electric-quadrupole transitions, is approximately equal to 4.10, which is the value for the ideal collective rotation.

Figure 2 : Intrinsic and laboratory fixed coordinate systems. The Euler angles (ϕ, θ, ψ) are denoted, collectively, by Ω . The curve expresses symbolically the intrinsic body, for which the deformation completely breaks the rotational symmetry.

Figure 3 : Rotational coupling scheme describing rotational motion of a spheroidal shape. The symmetry axis is labeled by S , the total angular momentum by \mathbf{I} and the collective

rotational angular-momentum by \mathbf{R} , while K is the projection of \mathbf{I} on S . Since \mathbf{R} must be perpendicular to S , $K = \Omega$, where Ω is associated with the intrinsic state ϕ_K .

Figure 4 : (a) Observed rotational bands in $^{166}_{68}\text{Er}_{98}$. Excitation energies (in MeV) of levels are written on the r.h.s., while the spin-parity $I\pi$ on the l.h.s. The levels belonging to a band are connected by strongly enhanced E2 transitions. The bands are labeled by the component K^π of the total angular momentum with respect to the symmetry axis ; $K^\pi = 0^+$ and 2^+ for the ground and the first excited bands, respectively. For $K=0$ R -symmetry implies a restriction on the I -values fulfilling the condition, $(-1)^I = r$. Consequently, only even- or odd- I values appear in a given rotational band. The ground state band of deformed even-even nuclei consists of even integer values of I with positive parity, since the configuration, in which a doubly degenerate time-reversed pair of one-particle levels in a deformed potential are pairwise filled, has $r=+1$. (b) Three lowest-lying rotational bands are observed in $^{238}_{92}\text{U}_{146}$. Due to R -symmetry of the deformation the rotational band with $K^\pi=0^-$ and $r = -1$ has members with $I^\pi = 1^-, 3^-, 5^-, \dots$, while the one with $K^\pi=0^-$ and $r = +1$ has those with $I^\pi = 0^-, 2^-, 4^-, \dots$

Figure 5 : Single-particle spectrum for an axially-symmetric harmonic-oscillator potential.

The energy eigenvalue of the one-particle orbit (n_x, n_y, n_z) is written as

$$\varepsilon(N, n_z) = \hbar\bar{\omega} \left(N + \frac{3}{2} - \frac{1}{3}\delta_{osc}(3n_z - N) \right) \quad (15)$$

where the principal quantum number $N = n_\perp (\equiv n_x + n_y) + n_z$ and $\bar{\omega} = (2\omega_\perp + \omega_z)/3$, while the deformation parameter δ_{osc} , which is approximately equal to $\beta \approx \delta$, is defined by

$$\delta_{osc} = 3 \frac{\omega_\perp - \omega_z}{2\omega_\perp + \omega_z} \approx \frac{R_z - R_\perp}{R_{av}}$$

where R_{av} denotes the mean radius. At $\delta_{osc} = 0$ (spherical shape) the spectrum is regularly bunched with the equal energy spacings $\hbar\omega_0$. Each major shell with the energy $(N + \frac{3}{2})\hbar\omega_0$ has the degeneracy $(N + 1)(N + 2)$ including the nucleon spin degree of freedom. The particle numbers, 2, 8, 20, 40, 70, 112, ..., would be the magic numbers for this potential and associated with an especially stable spherical shape. Single-particle levels belonging to a given major shell have the same parity $\pi = (-1)^N$

with the maximum orbital angular momentum $\ell_{max} = N$. For $\delta_{osc} \neq 0$ the levels split into $(N+1)$ levels with eigenvalues $\varepsilon(N, n_z)$ in (15), and each level has a degeneracy of $2(n_{\perp}+1)$, where a factor 2 comes from the nucleon spin $\frac{1}{2}$ while $(n_{\perp}+1)$ from possible values of $n_x (= 0, 1, 2, \dots, n_{\perp})$. For prolate (oblate) deformation, $\omega_z < \omega_{\perp}$ or $\delta_{osc} > 0$ ($\omega_z > \omega_{\perp}$ or $\delta_{osc} < 0$), the levels with larger (smaller) n_z become energetically lower. Eigenvalues expressed in units of the mean frequency $\bar{\omega}$ have a linear dependence on δ_{osc} , and the slope of the lowest level with a given N for prolate shape ($n_z = N$) is twice that for oblate shape ($n_z = 0$) with an opposite sign. The arrows mark the deformations corresponding to the indicated rational ratios of frequencies $\omega_{\perp} : \omega_z$. The figure gives the total particle number corresponding to completed shells in the potentials with $\omega_{\perp} : \omega_z = 1 : 1$ (spherical), $2 : 1$ (prolate) and $1 : 2$ (oblate). The figure is taken from Ref. [1].

Figure 6 : Observed low-lying level scheme of ^{25}Mg . Excitation energies of levels are expressed in units of MeV. The levels are mostly obtained from the reaction of ^{24}Mg (d, p γ) ^{25}Mg and, consequently, belong to the ^{24}Mg plus one-neutron configurations. In other words, only the one-particle levels lying higher than the $[202\ 5/2]$ level for prolate shape in the Nilsson diagram of Figure 7 are surely observed. The parameters in the expression (6), A for $K \neq 1/2$ bands (A and a for $K=1/2$ bands), which are estimated using the energies of the lowest two (three) rotational members, are indicated below respective bands. It is seen that already around band heads the rotational spectra of $K=1/2$ bands often deviate considerably from the $I(I+1)$ dependence. The decoupling parameters, which are estimated using respective $\Omega = 1/2$ particle wave functions in the spheroidal potential with $\beta \approx 0.4$, exhibit the characteristic behavior depending on different bands and are found to provide a further support for the assignment of the intrinsic configurations given in the figure [1].

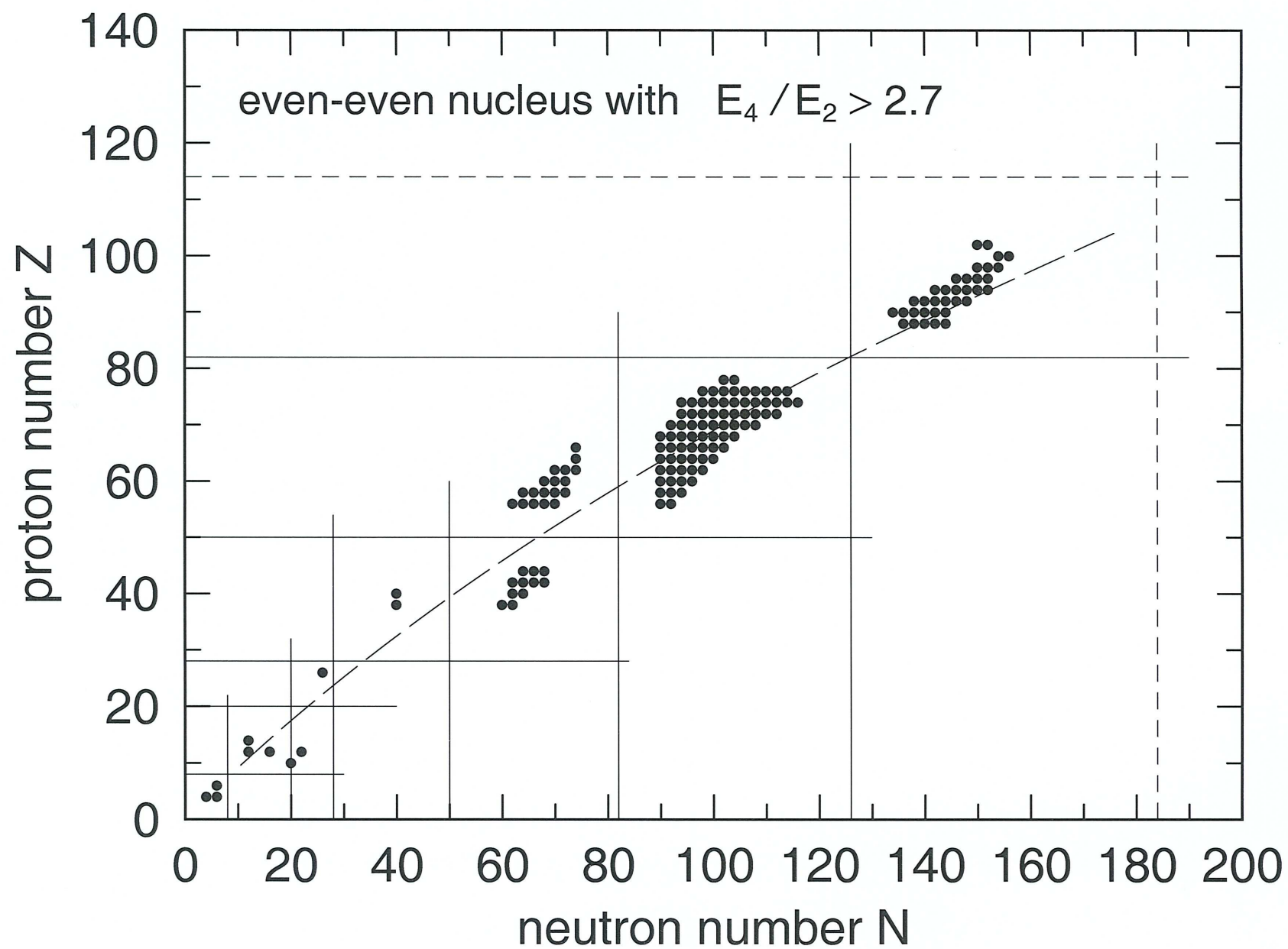
Figure 7 : Neutron one-particle levels in a spheroidal Woods-Saxon plus spin-orbit potential, for which the radius R and the depth V_{WS} are adjusted approximately to those of $^{25}_{12}\text{Mg}_{13}$. The parameters of the potential at $\beta=0$ are taken from p.239 of Ref. [29]. Positive-parity one-particle levels are denoted by solid curves. One-particle levels with $\varepsilon_{\Omega} > 0$ are obtained as one-particle resonant levels in the potential. The associated resonant widths are not shown, for simplicity. Calculated one-particle resonant ener-

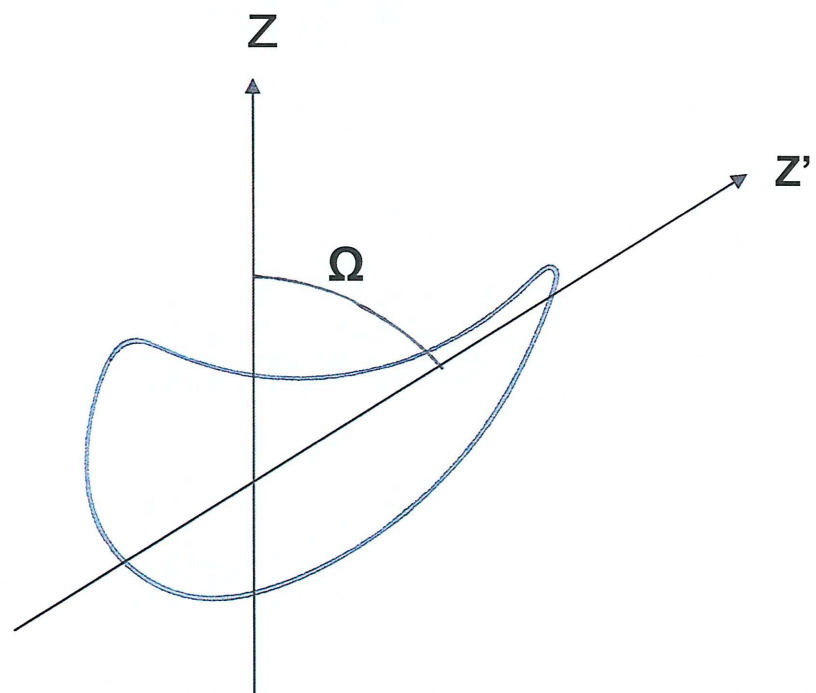
gies in MeV at $\beta=0$ are : $\varepsilon_{res}(p_{3/2})=0.32$, $\varepsilon_{res}(f_{7/2})=0.33$, and $\varepsilon_{res}(f_{5/2})=10.37$, while the $p_{1/2}$ level expected just above the $p_{3/2}$ and $f_{7/2}$ levels is not obtained as a resonant level for the present potential. Bound one-particle levels are labeled by the asymptotic quantum numbers $[Nn_z\Lambda\Omega]$, where Ω represents the component of the total angular momentum along the symmetry axis and is a constant of the motion for all values of β . The additional quantum numbers refer to the structure of the orbits in the limit of large deformations : the total number of nodal surfaces (N), the number of nodal surfaces along the symmetry axis (n_z), and the component of orbital angular momentum along the symmetry axis (Λ). Each level is doubly degenerate ($\pm\Omega$) associated with time reversed invariance of the Hamiltonian. The neutron numbers 16 and 20, which are obtained by filling in all lower-lying levels, are indicated with circles. A pairwise filling of the doubly degenerate ($\pm\Omega$) orbits contributes no net angular momentum along the symmetry axis. For example, in $^{25}\text{Mg}_{13}$ with the neutron number 13 it is seen that the lowest two intrinsic configurations for $\beta \approx 0.4$ are expected to involve the 13th neutron occupying the orbits $[202\ 5/2]$ and $[211\ 1/2]$, in agreement with the observed spectroscopic properties shown in Figure 6. The observed second and third excited bands starting at 2.563 and 3.413 MeV (Figure 6) can be interpreted as having the $[200\ 1/2]$ and $[330\ 1/2]$ intrinsic configurations, respectively, for the odd neutron.

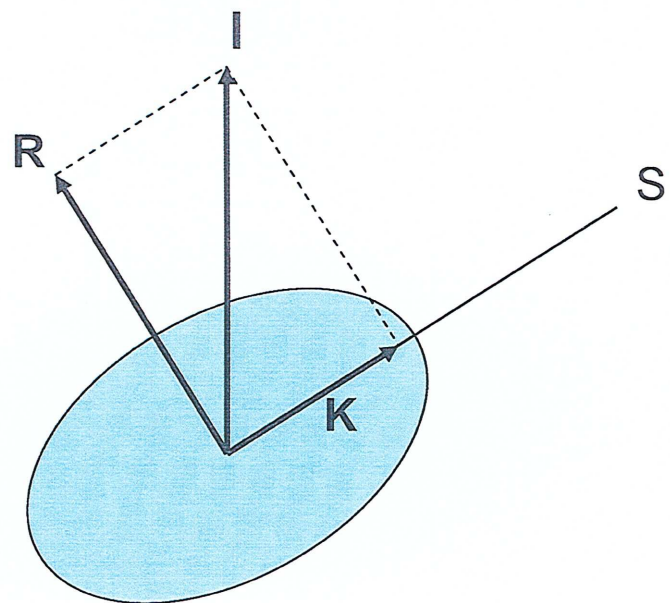
Figure 8 : Observed low-lying rotational bands of $^{175}_{70}\text{Yb}_{105}$. Excitation energies of levels are expressed in units of MeV. The levels which are observed by (d,p) reactions and thus classified as particle states are drawn to the right of the ground-state band $[514\ 7/2]$, while hole states observed by (d,t) reactions are drawn to the left. Only a few lowest-lying members are plotted for each rotational band, for simplicity. The classification of the intrinsic states is supported by the observed intensities in one-neutron transfer reactions, observed rotational energies and transition probabilities. See Ref. [1] for the detailed analysis. The data are taken from Nuclear Data sheets, **102** (2004) 719 and <http://www.nndc.bnl.gov/chart/>.

Figure 9 : Neutron one-particle levels in a spheroidal Woods-Saxon plus spin-orbit potential, for which the radius R and the depth V_{WS} are adjusted approximately to those of $^{175}_{70}\text{Yb}_{105}$. The parameters of the potential at $\beta=0$ are taken from p.239 of Ref. [29], except the strength of the spin-orbit potential that is about 20 percent stronger here.

The neutron numbers, 82, 104 and 126, which are obtained by filling in all lower-lying levels, are indicated with circles. It is seen that in the deformation region of $0.15 < \beta < 0.36$ the 105th neutron occupies the $[514\ 7/2]$ level, in agreement with the observed ground-state configuration of ^{175}Yb . Moreover, the observed sequence of intrinsic states shown in Figure 8 is seen to be consistent with the single-particle spectrum in the present figure at $\beta \approx 0.28$: in particular, above the $[514\ 7/2]$ level we find the $[624\ 9/2]$, $[510\ 1/2]$, $[503\ 7/2]$, $[512\ 3/2]$ and $[651\ 1/2]$ levels, while below the $[514\ 7/2]$ level we have the $[512\ 5/2]$, $[633\ 7/2]$ and $[521\ 1/2]$ levels. In the figure only the one-particle levels, which lie in the neighborhood of the $[514\ 7/2]$ level at $\beta=0.28$, are marked by respective asymptotic quantum numbers $[Nn_z\Lambda\Omega]$.







(16+) — 2.967

14+ — 2.389

12+ — 1.847

10+ — 1.350

8+ — 0.911

6+ — 0.546

4+ — 0.265

2+ = 0.081

0+ = 0.0

$K\pi = 0+$

$r = +1$

(14+) — 2.880

(13+) — 2.654

(12+) — 2.429

(11+) — 2.189

10+ — 1.964

9+ — 1.751

8+ — 1.556

7+ — 1.376

6+ — 1.216

5+ — 1.075

4+ — 0.956

3+ — 0.859

2+ — 0.786

$K\pi = 2+$

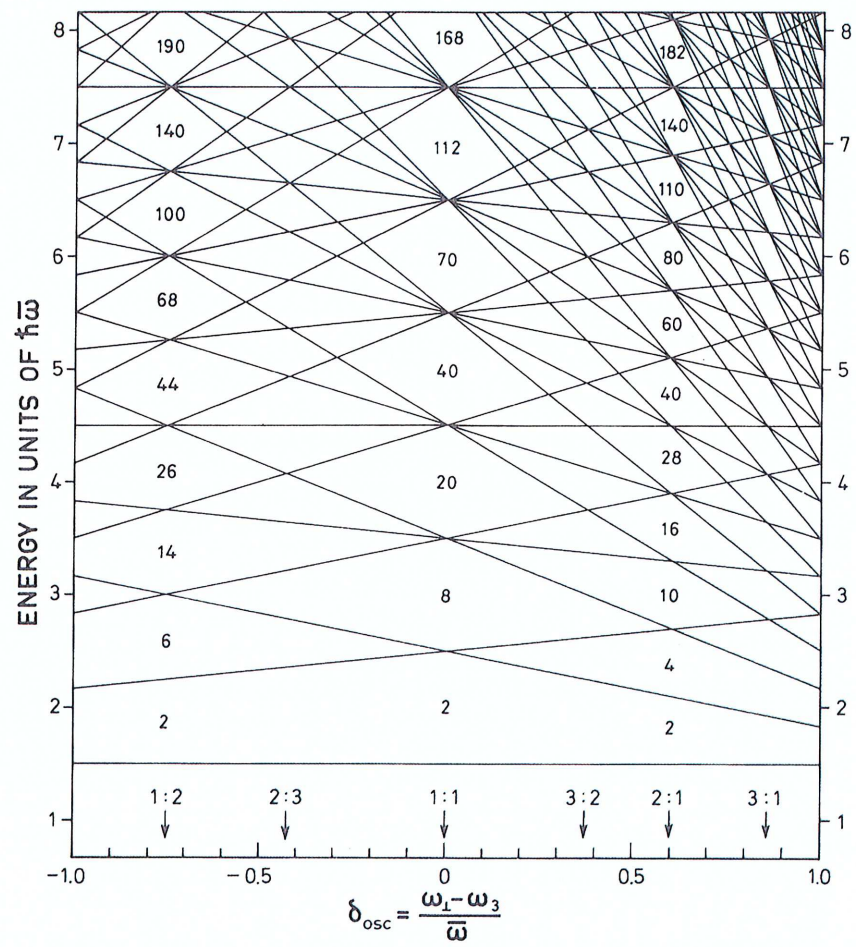
$^{166}_{68}\text{Er}_{98}$

30+ — 5.035
 28+ — 4.517
 26+ — 4.018
 24+ — 3.535
 22+ — 3.068
 20+ — 2.619
 18+ — 2.191
 16+ — 1.788
 14+ — 1.416
 12+ — 1.077
 10+ — 0.776
 8+ — 0.518
 6+ — 0.307
 4+ — 0.148
 2+ 0+ — 0.0 0.045
 $K\pi = 0+$
 $r = +1$

31- — 5.513
 29- — 5.003
 27- — 4.504
 25- — 4.017
 23- — 3.548
 21- — 3.104
 19- — 2.689
 17- — 2.307
 15- — 1.959
 13- — 1.649
 11- — 1.379
 9- — 1.151
 7- 5- 3- 1- — 0.827 0.966
 — 0.680 0.732
 $K\pi = 0-$
 $r = -1$

28- — 4.895
 26- — 4.424
 24- — 3.971
 22- — 3.538
 20- — 3.128
 18- — 2.744
 16- — 2.389
 14- — 2.066
 12- — 1.778
 10- — 1.528
 8- — 1.318
 6- — 1.151
 4- 2- — 0.950 1.028
 $K\pi = 0-$?
 $r = +1$

$^{238}_{92}\text{U}_{146}$



5.53 (11/2)

4.712 9/2

5.012 7/2

4.277 1/2
3.971 7/2

3.405 9/2

3.908 5/2

3.413 3/2

2.738 7/2

2.801 3/2
2.563 1/2

K π = 1/2-
[330 1/2]

1.964 5/2

K π = 1/2+
[200 1/2]

A = 0.113
a = -3.54

1.612 7/2

A = 0.150
a = -0.47

0.975 3/2

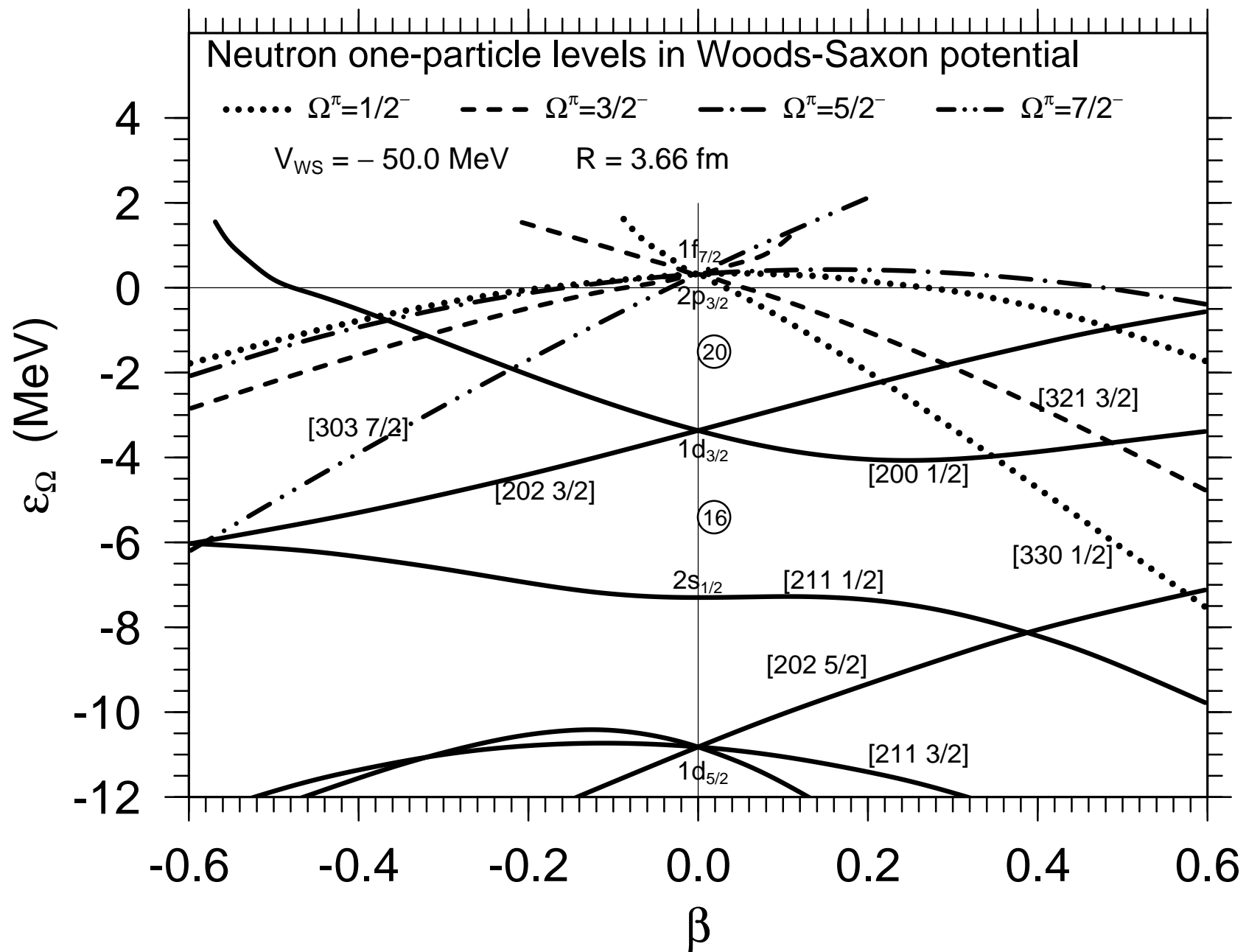
0.585 1/2

0 5/2

K π = 5/2+
[202 5/2]
A = 0.231

K π = 1/2+
[211 1/2]
A = 0.163
a = -0.020

²⁵Mg₁₃



1.469 — (3/2+)
 1.368 — (5/2+)
 1.356 — (1/2+)

1.174 — 7/2-

[651 1/2] ?

1.009 — (5/2-)
 0.992 — 3/2-
 0.920 — 1/2-

0.957 — (7/2)-
 0.872 — (5/2)-
 0.811 — (3/2)-

0.844 — (9/2-)
 0.729 — (7/2)-
 0.639 — (5/2)-

0.698 — 7/2-
 0.603 — 5/2-
 0.556 — 3/2-
 0.515 — 1/2-

[521 1/2]

0.524 — (13/2)+

[512 3/2]

[512 5/2]

0.385 — (11/2+)

[510 1/2]

0.268 — (9/2+)

0.232 — (11/2-)

0.105 — (9/2)- [624 9/2]

0.0 — (7/2-)

[514 7/2]

¹⁷⁵₇₀Yb₁₀₅

